THE ASTROPHYSICAL JOURNAL, 446:692–698, 1995 June 20

AMMONIA OBSERVATIONS OF NGC 6334 I(N)

T. B. H. KUIPER
Jet Propulsion Laboratory 169-506, California Institute of Technology, Pasadena, CA 91109
W. L. PETERS III
Steward Observatory, University of Arizona, Tucson, AZ 85721
AND
J. R. FOSTER,[1] F. F. GARDNER, AND J. B. WHITEOAK
Australia Telescope National Facility, Commonwealth Scientific and Industrial Research Organization, P.O. Box 76, Epping, NSW, 2121, Australia
Received 1993 March 12; accepted 1995 January 4

ABSTRACT

Coincident with the far-infrared source NGC 6334 I(N) and water maser source E is a massive dense cloud which has the most intense ammonia (1, 1) emission of any known interstellar cloud. We have mapped the (3, 3) emission and find the cloud is extended 0.8 pc in the direction parallel to the Galactic plane, and 0.5 pc perpendicular to it. It has a velocity gradient of 1 km s^{-1} pc^{-1} perpendicular to the Galactic plane. The gas kinetic temperature is about 30 K and the density is greater than 10^6 cm^{-3}. The mass of the cloud is about 3000 $M_\odot$, 3 times greater than previously estimated. The para-ammonia column density is 6–8 × 10^{15} cm^{-2}. An ammonia abundance of 0.5–1.5 × 10^{-8} is inferred, where the larger number assumes an early time ortho/para ratio. This suggests either a cloud age of less than $\sim 10^6$ yr, or substantial depletion of ammonia.

Subject headings: ISM: individual (NGC 6334) — radio lines: ISM

1. INTRODUCTION

NGC 6334 is described by Herschel as a large, faint, irregular nebulosity (Dreyer 1962). In the far-infrared, it consists of a string of sources extending about a degree along the Galactic plane, and lying about half a degree above it. Moran & Rodriguez (1980) have suggested that the NGC 6334 complex contains examples of various stages of star formation. They proposed that NGC 6334 I(N)[2] is an example of the earliest, pure accretion phase, prior to the formation of a star. This object is not visible in the far-IR shortward of about 130 μm (Loughran et al. 1986), but is the most prominent source in the region at 1 mm (Cheung et al. 1978; Gezari 1982).

This region has a very high column density, about 10^{24} cm^{-2} (Cheung et al. 1978) and is the brightest known source of ammonia (1, 1) emission in the sky (Forster et al. 1987, hereafter FWGPK). There are also class I methanol masers (Menten & Batrla 1989; formerly called class A, Menten 1991) which are associated with dense cores without the energetic phenomena associated with newly formed stars. The thermal methanol lines in this source also indicate a low temperature ($\sim$20 K; Menten & Batrla 1989). However, the 22 GHz water maser at the center indicates at least localized high density and temperature (about 10^9–10^{10} cm^{-3} and 200–300 K).

An interesting contrast is presented by NGC 6334 I, about 2 arcmin south of I(N), which Moran & Rodriguez (1980) suggest represents the second stage in which a stellar core has formed and a star has just turned on. This object is the most prominent in the region at 100 μm (Gezari 1982; Loughran et al. 1986). It is far less prominent at 1 mm (Cheung et al. 1978) and has less than half the column density of I(N). It does not stand out in the ammonia (1, 1) transition (FWGPK), but high resolution observations show compact structure which is consistent with a dense disk or toroid (Jackson, Ho, & Haschick 1988). There are water and OH masers (Moran & Rodriguez 1980; Raimond & Eliasson 1969) and a compact H II region (Rodríguez, Cantó, & Moran 1982) at this location. There are also class B methanol masers, usually associated with compact H II regions (Menten & Batrla 1989), including the strongest known 12.1 GHz maser (Batrla et al. 1987). The thermal methanol lines in this region indicate a higher temperature of 36 K (Menten & Batrla 1989).

We previously used the Parkes radio telescope to map the region of the NGC 6334 complex (FWGPK). Both the (1, 1) and (2, 2) transitions were observed. The (1, 1) map shows an intense peak at the position of water maser source E (Moran & Rodriguez 1980). It is, in fact, the most intense source of ammonia (1, 1) emission known to us. We report here additional observations of the (2, 1), (3, 3), and (6, 6) transitions and a new analysis to investigate the nature of the source NGC 6334 I(N).

2. OBSERVATIONS

We used the NASA Deep Space Network 64 m tracking antenna (now a 70 m antenna) near Canberra, Australia, to map NGC 6334 I(N) in the (3, 3) (23,870.192 MHz) transition and to observe (2, 1) (23,098.819 MHz) and (6, 6) (25,056.025 MHz) transitions. The observations were conducted during six sessions between 1986 October 13 and 1986 October 30, and took about 30 hours of antenna time, including calibrations. Prior to the antenna's upgrade, its efficiency at 24 GHz was quite low, about 6%. The beamwidth was measured to be 55″.

The data are presented in Table 1. The positions are right ascension and declination offsets in arcsec relative to a nominal map center of $17^h17^m34^s$, −35°41′50″. The antenna temperatures have been corrected for antenna gain as a function of elevation and for atmospheric absorption.

Figure 1 shows a map of the corrected antenna temperature. The filled circles in Figure 1 show the positions at which data

[1] Now at Hat Creek Radio Observatory, University of California at Berkeley, Route 2 Box 500, Cassel, CA 96016.
[2] For a review of the nomenclature, please refer to the Appendix.

TABLE 1

(3, 3) OBSERVATIONS OF NGC 6334 I(N)

Offset		T_A^*	V_{LSR}	Line FWHM
R.A.	Decl.	(K)	(km s^{-1})	(km s^{-1})
0″	+29″	9.04 ± 0.37	−4.27 ± 0.08	3.75 ± 0.18
+58	0	7.94 ± 0.41	−4.06 ± 0.12	4.79 ± 0.28
+29	0	14.70 ± 0.37	−4.39 ± 0.05	4.47 ± 0.13
0	0	13.31 ± 0.30	−4.17 ± 0.03	4.06 ± 0.07
−29	0	7.93 ± 0.41	−4.25 ± 0.12	4.38 ± 0.27
+58	−29	6.73 ± 0.58	−4.80 ± 0.17	3.75 ± 0.39
+29	−29	18.30 ± 0.45	−4.56 ± 0.05	4.32 ± 0.12
0	−29	19.01 ± 0.38	−4.26 ± 0.04	4.40 ± 0.10
−29	−29	11.69 ± 0.57	−4.01 ± 0.10	4.23 ± 0.24
+29	−58	11.94 ± 0.44	−4.72 ± 0.08	3.03 ± 0.18
0	−58	13.79 ± 0.43	−4.45 ± 0.06	4.42 ± 0.15
0	−86	6.74 ± 0.37	−5.05 ± 0.12	4.51 ± 0.28

were taken. The contours are at 2 K intervals. The antenna half-power beamwidth is shown in the lower left corner. There is evidence for a velocity gradient across the cloud. Figure 2 shows a contour plot of the LSR velocity of the (3, 3) transition.

We also observed the ammonia (2, 1) (23,098.819 MHz) and (6, 6) (25,056.025 MHz) transitions at the nominal map center where the (3, 3) emission is about 75% of its peak value (Fig. 3 and Table 2). The dashed lines represent Gaussian fits to the data, after a baseline correction was applied. A simple Gaussian, which ignores hyperfine structure, is appropriate because the (2, 1) data, which should show the same hyperfine structure as the (2, 2) line (see Fig. 4), are too noisy to justify fitting the hyperfine ratio, and because the (3, 3) and (6, 6) lines have 89% and 97%, respectively, of their power in the main component.

The Parkes 64 m telescope was used to observe the (1, 1) (23,694.496 MHz) and (2, 2) (23,722.633 MHz) transitions during a project to map the entire NGC 6334 complex (FWGPK). The spectra obtained at I(N) and the fitted profiles are shown in Figure 4. The general fitting procedure has been described by Kuiper et al. (1984) and its application to ammonia by Kuiper et al. (1987). Corrected for antenna efficiency and atmospheric absorption, the results of fitting the profiles are given in Table 2. The optical depths refer to the main hyperfine component, designated by $\tau(J, K; m)$.

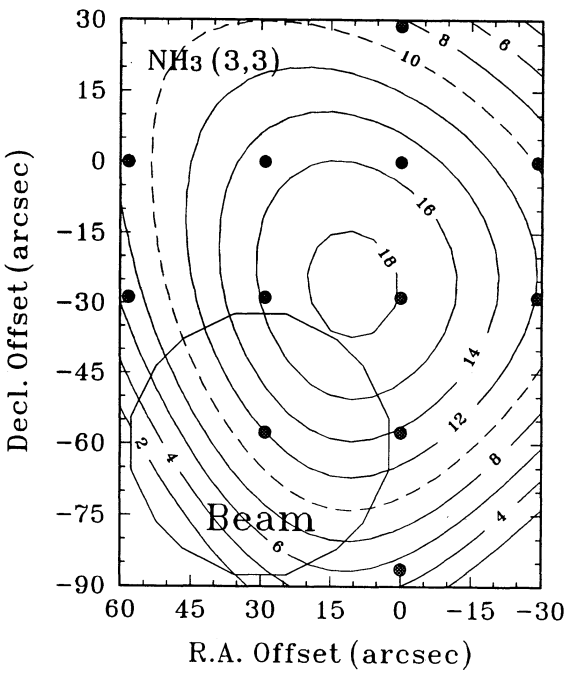

FIG. 1.—Corrected (3, 3) antenna temperature map of NGC 6334 I(N), centered at 17^{h}17^{m}34^s, −35°41′50″. The contours are at 10%–90% of the peak emission. The dashed contour represents 50% emission.

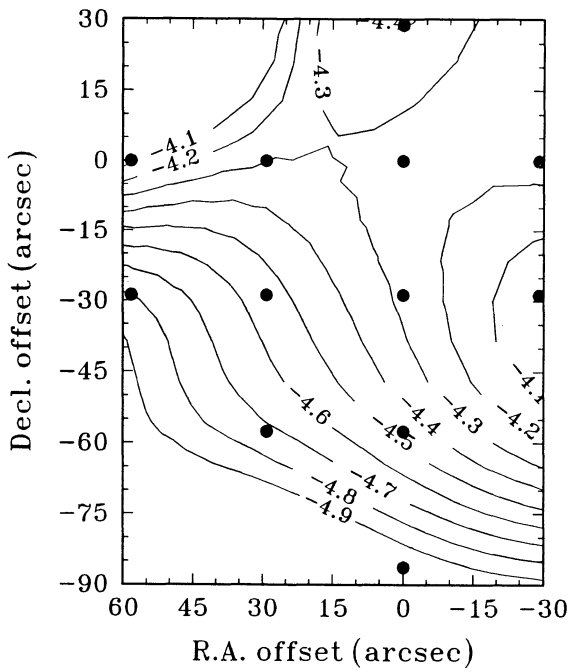

FIG. 2.—Velocity of the (3, 3) transition with respect to the local standard of rest is plotted on the same scale as Fig. 1. The contour interval is 0.1 km s^{-1}.

3. ANALYSIS

It is common practice to analyze observations such as these in terms of *average* physical conditions—kinetic temperature, H_2 density, and NH_3 column density. The implicit homogeneous source model is probably not physically realistic and it is

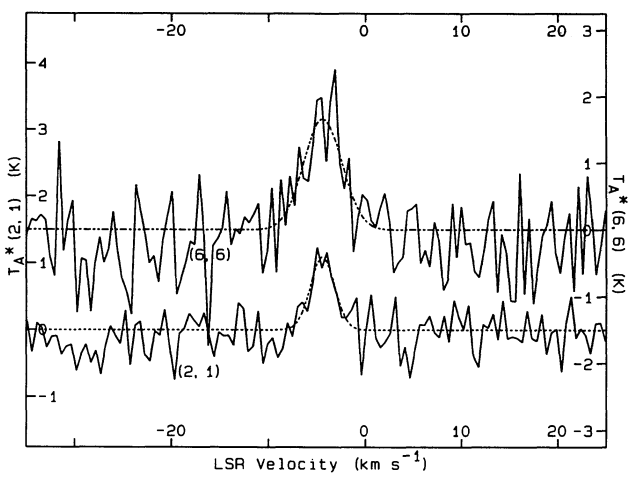

FIG. 3.—Spectra of the (2, 1) and (6, 6) emission observed at the nominal map centre position, i.e., at about the 79% contour level of the (3, 3) line.

TABLE 2

OBSERVED AMMONIA LINE PARAMETERS

Transition (J, K)	T_A^* (K)	V_{LDR} (km s^{-1})	FWHM (km s^{-1})	$\tau(J, K; m)$	Antenna
Observed at 17^{h}17^{m}35^s, −35°42′17″ (1950.0)					
(1, 1).....	13.2 ± 0.4	−4.97 ± 0.02	2.96 ± 0.04	1.69 ± 0.09	Parkes
(2, 2).....	9.1 ± 0.75	−4.92 ± 0.02	3.05 ± 0.05	1.07 ± 0.13	Parkes
Observed at 17^{h}17^{m}34^s, −35°41′50″ (1950.0)					
(2, 1).....	1.1 ± 0.2	−4.9 ± 0.2	2.9 ± 0.5		Canberra
(3, 3).....	13.3 ± 0.2	−4.2 ± 0.03	4.1 ± 0.1		Canberra
(6, 6).....	1.7 ± 0.4	−4.9 ± 0.9	4.6 ± 2.0		Canberra

understood that the average conditions obtained are weighted toward those regions whose physical conditions favor the emission and escape of radiation. A filling factor expresses the possibility of clumpy source structure. We will use such a simple model as our starting point and then elaborate on it as the data require. Such a procedure should give more confidence in the uniqueness of the interpretation than to present a more elaborate model which is consistent with the data but whose uniqueness might be hard to establish.

The standard methods of analysis of NH_3 inversion transition observations (e.g., Martin & Barrett 1978; Ho et al. 1979; Walmsley & Ungerechts 1983) assume relatively low excitation of the J-ladders (i.e., low $n(H_2) \times N(NH_3)$ and are not appropriate for a source as bright as this (Stutzki & Winnewisser 1985b). As discussed in detail below, we estimated the kinetic temperature, H_2 density, and NH_3 column density by comparing line intensity ratios and optical depths, which are to first-order independent of filling factor, to the corresponding observed quantities calculated from simple source models using the two-temperature partition function method described by Kuiper (1994). The filling factor was then estimated by comparing the predicted and observed brightness temperatures.

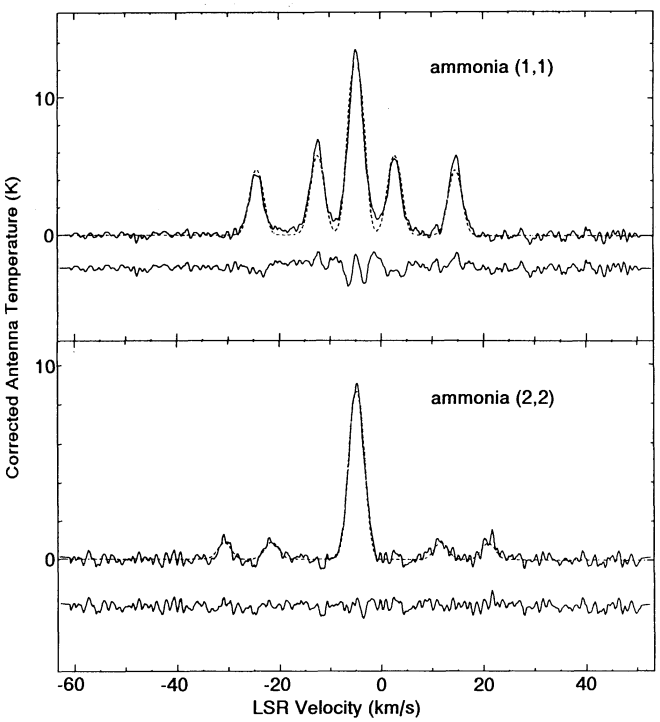

FIG. 4.—Spectra of the (1, 1) and (2, 2) emission at I(N). The fitted line profiles are shown as dashed lines, with the residuals below the observed spectra. The temperature scale has been corrected for efficiency and atmospheric absorption.

To make the comparison, some corrections were applied to the observations for the different beam sizes and positions:

FWGPK determined that the source is 144″ long by 84″ wide in the (1, 1) transition, corrected for the 84″ beamwidth of the Parkes radio telescope. If the source is not clumpy, then this implies a beam dilution, $\Phi(1, 1)$, of 0.63. The central brightness temperature of the source in the (1, 1) transition is then 21.0 ± 0.6 K.

The (3, 3) mapping data were fitted to an elliptical Gaussian function. The best fit was obtained for a gaussian 110″ long by 83″ wide, with the major axis having a position angle of 120°. Thus, the cloud is roughly aligned with the entire NGC 6334 complex, and with the Galactic plane. A peak T_A^* of 19.5 K was located at 17^{h}17^{m}35^s, −35°42′17″, exactly on top of H_2O maser source E (Moran & Rodriguez 1980). Assuming Gaussian source and beam shapes, the actual (3, 3) source is estimated to be 95″ long and 62″ wide. The beam dilution amounts to 0.66, giving an actual peak brightness temperature of 29.5 ± 3 K.

In our observations of the (2, 1) transition we obtained a corrected antenna temperature of 1.1 ± 0.2 K at a position 30″ north by northwest of the center of the source where the fitted Gaussian is 79% of its peak value. If the (2, 1) source were the same size and at the same position as the (1, 1) source then the corrected antenna temperature in the (2, 1) transition would be ~1.4 K at the source center. On the other hand, if the (2, 1) source were the same size as the (1, 1) source, the intensity at this position would be 90% of the central intensity, and the central antenna temperature would be 1.2 K. In view of the uncertainty of these assumptions and the error inherent in the measurement, we estimate that the peak (2, 1) antenna temperature is between 1.0 and 1.6 K.

3.1. *Para-ammonia*

To obtain the physical conditions (T_k, $n(H_2)$, and $N(NH_3)$ we used the ratio of the (2, 2) and (1, 1) line intensities, = 0.69 ± 0.06, the ratio of the (1, 1) and (2, 1) lines (9.6 ± 1.4), and the (1, 1) and (2, 2) optical depths (Table 2). In our calculations, we used the collision rates by Danby et al. (1987).

In the case of a homogeneous spherical model, treated by Stutzki & Winnewisser (1985), if the beam size is much larger than the size of the source, the observations should be compared to compute quantities which are averages over the

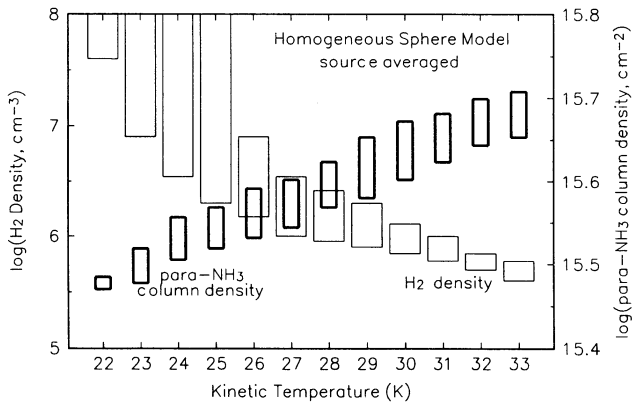

FIG. 5.—Ranges of $n(H_2)$ and N(para-NH_3) where the source-averaged values of $T_B(2, 2)/T_B(1, 1)$, $T_B(1, 1)/T_B(2, 1)$, $\tau(1, 1)$, and $\tau(2, 2)$ agree to within 1 σ to the observed values are shown as a function of T_k, the kinetic temperature, for the homogeneous sphere model.

source. When the source is much larger than the beam, the comparison should be with values computed for the center of the source. Since our case in intermediate between these, we considered both.

For a range of values of T_k, we made contour plots of $T_B(1, 1)$, $\tau(1, 1)$, $\tau(2, 2)$, $T_B(2, 2)/T_B(1, 1)$, and $T_B(1, 1)$, and $T_B(1, 1)/T_B(2, 1)$ computed for 10^4 cm$^{-3} \leq n(H_2) \leq 10^8$ cm^{-3} and $10^{14.5}$ cm$^{-2} \leq N$(para-NH_3) $\leq 10^{16.5}$ cm^{-2}, averaged over a homogeneous sphere. The average optical depth is 1.5 times the optical depth along the radius. In the plots which correspond to values of T_k from 22 K and 33 K, we found that there was simultaneous overlap of the 1 σ ranges of the four observed quantities $\tau(1, 1)$, $\tau(2, 2)$, $T_B(2, 2)/T_B(1, 1)$, and $T_B(1, 1)/T_B(2, 1)$. The range of T_k, $n(H_2)$ and N(para-NH_3) for which such "solutions" exist is shown in Figure 5. At the lower values of T_k the observational data only set a lower limit on $n(H_2)$, which indicates that under these conditions the ammonia rotational energy levels are almost fully thermalized. It is interesting that the temperature which describes the populations within the J-ladders, T_J (see Kuiper 1994), is approximately 22 K for the entire range of T_k for which there are solutions. The averaged brightness temperatures, computed using equation (A4) of Stutzki & Winnewisser (1985a), are shown in Figure 6 as a function of T_k. The solutions for $T_k = 29$ K predict an average $T_B(1, 1)$ over the sphere which corresponds to our observed corrected antenna temperature, $T_A^* = 13.2$ K. For this solution, $n(H_2) = 0.8$–2×10^6 cm^{-3}. Solutions with higher T_k (up to 33 K) and unresolved, slightly clumpy structure are consistent with our data, but those with lower T_k predict a source which is not bright enough. The para-NH_3 column density, defined along the radius of the source, is pretty much the same in all cases, 3–5 $\times 10^{15}$ cm^{-3}.

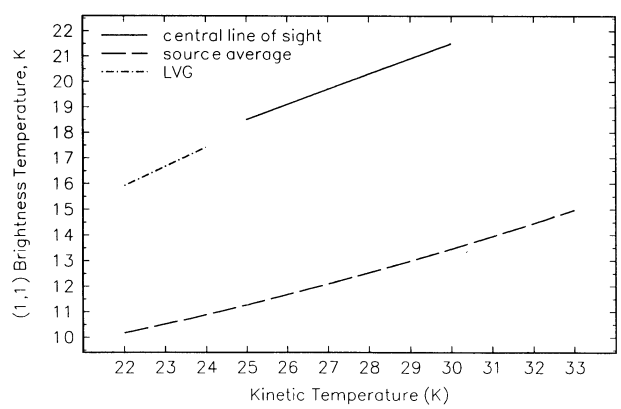

FIG. 6.—Brightness temperatures, computed from the various models discussed in the text for the values of T_k, $n(H_2)$ and N(para-NH_3) which correspond to the observations, are plotted as a function of T_k.

The results of the calculation for values along the central line of sight of a homogeneous spherical cloud constrain the values of T_k to the range of 25–30 K. In this case, the observed optical depth is twice the optical depth along the radius. The brightness temperatures are calculated with the usual formula (e.g., eq. (1) in Stutzki & Winneweisser 1985b). For $T_k = 29$–30 K, the computed central brightness temperature (see Fig. 6) agrees with our estimate of 21 $\pm$ 0.6 K. The density required at this temperature is slightly lower, 5–8 $\times 10^5$ cm^{-3}. The para-ammonia column density (defined along the radius) is also slightly lower, 2.6–3 $\times 10^{15}$ cm^{-2}, with the higher value corresponding to the higher T_k.

To get a feeling for the effect of source geometry on the results of the calculation, we also considered the traditional spherical large velocity gradient formalism, as expressed in an escape probability of the form $\beta(\tau) = [1 - \exp(-\tau)]/\tau$. In this case we found the range of possible T_k to be 22–24 K, with $n(H_2)$ in the range of 0.3–3 $\times 10^7$ cm^{-3}, and a para-NH_3 column density, now defined as going through the source instead of only to the center, of 4.5–5 $\times 10^{15}$ cm^{-3}. However, the computed (1, 1) brightness temperature is then only 16–18 K, which is too low to be consistent with our observations. For the LVG case with planar geometry (in which 3τ replaces τ in the above equations for β), the results are the same except that the minimum H_2 density is reduced by a factor of 3.

In summary, the para-ammonia emission appears to arise from region which nearly fills the Parkes 84″ beam, shows negligible clumping, has an average kinetic temperature of about 29 K, a average gas density of about 10^6 cm^{-3}, and a para-ammonia column density *through* the source of 6–8 $\times 10^{15}$ cm^{-2}.

3.2. *Ortho-ammonia*

The (3, 3) brightness temperature, 30 $\pm$ 3 K, obtained from the antenna temperature by correcting for position and source size as discussed in the previous section, is larger than the (1, 1) brightness temperatures and comparable to the (1, 1) excitation temperature and the kinetic temperature. This implies that (1) the transition is inverted (is a maser), or at least the (3, 3) excitation temperature is higher than the kinetic temperature, or (2) the (3, 3) optical depth is very high, or (3) the kinetic temperature is higher in the region where the (3, 3) emission arises. We argue that a higher kinetic temperature is the most likely explanation.

There is a mechanism by which the (3, 3) inversion doublet could be super thermally excited or even inverted. The collision rates for ortho-NH_3 with para-H_2 (Danby et al. 1986) preferentially excite the upper level of the (3, 3) doublet (Flower, Offer, & Schilke 1990). Observations have for some time suggested that over-population or even inversion of the (3, 3) doublet does arise under certain suitable conditions such as those found in DR 21 (Guilloteau et al. 1983) and W28 A2 (Gómez et al. 1991). Maser emission was unambiguously observed in the (3, 3) transition at the position of the western methanol masers DR 21 (OH) main (Mangum & Wootten 1994).

In all cases of enhanced (3, 3) emission, the physical condi-

tions are quite different from those found in NGC 6334 I(N). The DR 21, the emission arises from a warm ($\sim$70 K) cloud in front of a continuum source (Guilloteau et al. 1983) where the (1, 1) and (2, 2) lines are seen in absorption. W28 A2, Gómez et al. (1991) have noted is, similar to NGC 6334 IV, a compact bipolar ionized outflow region with a warm ($\sim$90 K) molecular envelope, where the (2, 2) emission is also seen in absorption against the continuum. The comparison with DR 21 (OH) is more interesting. The methanol masers in this source are class I, like the one observed by Menten & Batrla (1989) in NGC 6334 I(N). However, the sources' morphologies suggest that the cases are not similar. In DR 21 (OH) main, the extended NH_3 (3, 3) emission peaks at the same position as the NH_3 (1, 1) and (2, 2) emission, the CS 2–1 emission, and the mm continuum. The NH_3 emission however also shows extensions towards the CH_3OH maser positions, and an unresolved bright peak at the position of the western CH_3OH maser, well away from the molecular peak. This suggests that these CH_3OH and NH_3 (3, 3) masers occur in lower density gas. There is also evidence that they occur in gas that is warmer than the average for I(N). The A-state methanol masers lie approximately 45 and 55 cm^{-1} (65 and 80 K) above the ground state. Flower et al. (1990) and Mangum & Wootten (1994) have modeled the excitation and find that temperatures $\geq$100 K and densities less than 10^5 cm^{-3} are implied. While a larger map of the (3, 3) emission in I(N) might possibly reveal peripheral maser spots, it is not expected in the dense cool core we have mapped. We therefore consider possibility (1) unlikely.

We next consider possibilities (2) and (3), high τ or $T_k > 30$ K. In comparing a transition of ortho-ammonia to one of para-ammonia, we may need to treat the two species as essentially different molecules, because the timescale for achieving equilibrium between the two species is very long, $\geq 10^6$ yr (Cheung et al. 1969). Therefore, the ratio of total (summed over hyperfine components) optical depths of the (3, 3) and (1, 1) transitions should be written as

$$\frac{\tau_{3,3}}{\tau_{1,1}} \simeq 7 \frac{N_{\rm ortho} \exp(-E_{3,3}/kT_{03})/Q_{\rm ortho}}{N_{\rm para}/Q_{\rm para}},$$

where N is the column density of the species, Q is the partition function referred to the lowest level of the species ($E_{0,0}$ for ortho, $E_{1,1}$ for para), and T_{03} is the rotation temperature which describes the relative populations of the (3, 3) and (0, 0) levels. In general, T_{03} is less than T_k (Walmsley & Ungerechts 1983). The factor 7 accounts for differences in the dipole moment matrix elements and the nuclear spin statistical weights. All approximately equal quantities such as frequency, doublet excitation temperature, and line width have been factored out.

We consider the nonequilibrium (early time) case first. In the absence of a mechanism to select H nuclei with a specific nuclear spin, one quarter of the molecules will be formed with all H nuclear spins aligned (para-ammonia), i.e., $N_{\rm ortho}/N_{\rm para} = 3$. At low temperatures, $Q_{\rm para}/Q_{\rm ortho} \simeq 3$, because only the lowest levels of the ortho $K = 0$ and para $K = \pm 1$ ladders are populated. The fact that there are two $|K| = 1$ ladders makes up for the fact that the nuclear spin statistical weight for ortho is double that for para. Thus, the degeneracy $2J + 1$ favors the para $|K| = 1$ ladders by a factor of 3. Hence

$$\frac{\tau_{3,3}}{\tau_{1,1}} \simeq 63 \exp\left(\frac{-123}{T_{03}}\right). \quad (1)$$

The following discussion shows that this is the highest expected optical depth ratio.

On a long enough timescale, the two species may achieve equilibrium. In that case, both partition functions should be referred to the (0, 0) level. Using the two temperature partition function of Kuiper (1994), one can show that the partition function summed over the para states is then

$$Q_{\Sigma\rm para} = Q_{\rm para} \exp(E_{1,1}/kT_k),$$

and, of course, $Q_{\Sigma\rm ortho} = Q_{\rm ortho}$. Then, the optical depth ratio becomes

$$\frac{\tau_{3,3}}{\tau_{1,1}} \simeq 7 \frac{N_{\rm ortho} \exp(-123/T_{03})/Q_{\Sigma\rm ortho}}{N_{\rm para} \exp(-23/T_k)/Q_{\Sigma\rm para}}. \quad (2)$$

As the two species approach equilibrium $N_{\rm ortho}/N_{\rm para} \rightarrow Q_{\rm ortho}/Q_{\rm para}$, and so we see that the early-time ratio expressed by equation (1) exceeds the equilibrium ratio, equation (2), for $T_k > 10.5$ K, and that for a warm cloud like I(N) the highest optical depth ratio occurs for an early-time ortho/para ratio.

In evaluating equation (1), we note that T_{03} may be as low as T_{12} (compare Figs. 2*a* and 2*b* of Walmsley & Ungerechts 1983) and, barring nonthermal excitation, as high as T_k. In the homogeneous spherical cloud approximation used in the previous section, we found T_{12} to be 22–24 K for the both cases. So, given 22 K $< T_{03} <$ 30 K, we find $0.24 < \tau_{3,3}/\tau_{1,1} < 1.04$ or $0.43 < \tau_{3,3;m}/\tau_{1,1;m} < 1.85$. If $T_{\rm ex}(3, 3) = T_{03} = 30$ K and, since $\tau_{1,1;m} = 1.7$, then $T_B(3, 3) = 29$ K, which is the observed value. However, as it is likely that T_{03} is less than T_k, it appears that the (3, 3) line is formed in a region where T_k and $T_{\rm ex}(3, 3)$ are higher than 30 K.

A lower $\tau(3, 3)$, higher $T_{\rm ex}(3, 3)$ solution is also possible in the equilibrium case (eq. [2] as $N_{\rm ortho}/N_{\rm para} \rightarrow Q_{\rm ortho}/Q_{\rm para}$). Still assuming that $T_{\rm ex}(3, 3) \leq T_k$, a simple radiative transfer solution implies that

$$\tau \geq \log\left[\frac{T_k}{T_k - (T_B - 2.7)}\right]$$

This yields values of $\tau(3, 3; m)$ which are consistent with equation (2) for $T_{03} \simeq$ 30–35 K and $T_k \geq 40$ K. Thus, without more observations to support a detailed model of the variation of T_k and $n(H_2)$, we cannot presently constrain the ortho/para ratio sufficiently to determine when the ammonia was formed within the last 10^6 yr.

The conclusion that there is a higher temperature core is reenforced by the observation of the (6, 6) line. The $T_A^*(6, 6)/T_A^*(3, 3)$ ratio can only be achieved with $T_k \geq 95$ K for ammonia in LTE. The complementary conclusion is that these warmer regions are hidden from our view in the lower metastable transitions by high optical depths.

It is perhaps pertinent to note at this point that (3, 3) and (6, 6) lines are slightly wider ($\sim$4 km s^{-1}) than the $K = 1$ and $K = 2$ lines (3 km s^{-1}) discussed earlier, pointing to a higher degree of turbulence in the inner cloud regions.

3.3. *Source Structure*

Direct and indirect measurements of source size show an increase in the density toward the center NGC 6334 I(N). The excitation temperatures of the (1, 1) and (2, 2) transitions are

equal for the conditions we have derived (e.g., Fig. 6 in Stutzki & Winnewisser 1985b or Fig. 2 in Kuiper 1994), and so since

$$\frac{\Delta T_A^*(2,2;m)}{\Delta T_A^*(1,1;m)} = \frac{\Phi(2,2)T_{\rm EX}(2,2)\{1-\exp[-\tau(2,2;m)]\}}{\Phi(1,1)T_{\rm EX}(1,1)\{1-\exp[-\tau(1,1;m)]\}},$$

where Φ is the fraction of the antenna beam filled by the source (beam dilution) and m refers to the main hyperfine component, we can conclude from the measured antenna temperatures and optical depths that $\Phi(2,2)/\Phi(1,1) = 0.85 \pm 0.08$, i.e., that the source is slightly smaller in the (2, 2) transition than in the (1, 1) transition. We observed the (3, 3) to be smaller still. This behavior is similar to what is observed in Ori MC1 (Ho et al. 1979); Wilson, Downes, & Bieging 1979; Ziurys et al. 1981). Thus, as one progreses to higher metastable levels with smaller optical depths the source becomes smaller, which is consistent with a centrally condensed density distribution.

3.4. *Cloud Mass*

At a distance of 1.7 kpc (Neckel 1978), the cloud observed in the (3, 3) transition is 0.8 by 0.5 pc. Observations by Gezari (1982) at 400 and 1000 μm show a source size of $\sim 50''$ (0.4 pc), comparable to the smaller dimension of the source in the (3, 3) transition. Since the source is optically thin in the far-IR, whereas the (3, 3) line probability has an optically thick core, these are also consistent with a central density condensation. Gezari used the dust opacity to estimate a gas column density of 10^{24} cm^{-2}. If the source depth is comparable to its apparent size, this implies a density of 3×10^5 cm^{-3} and a mass of 1000 $M_\odot$, comparable to such sources as W3 and DR 21. Our density estimate above suggests that this it is probably at least 3000 $M_\odot$. Averaged over the source, Gezari obtained $T = 23 \pm 5$ K, $\tau(400\ \mu\text{m}) = 0.3$, and an emissivity index $n \simeq 2$. Thus, $\langle \tau(100\ \mu\text{m}) \rangle \approx 4$–5. If the source is centrally condensed, there may be a substantial amount of material present which is not visible at 100 μm, only barely visible at 400 μm, and so on. This would cause underestimates of T and τ, so that Gezari's data are not inconsistent with our higher mass estimate.

Consideration of the virial theorem suggests that the cloud is in equilibrium or contracting. If we take the average radius of the cloud as seen in (3, 3) emission to be 0.33 pc, then the line width of 4 km s^{-1} implies that if the mass exceeds 2500 $M_\odot$ the cloud is self-gravitating. This is higher than the estimate of FWGPK because the line width is larger and the source size is smaller. If the velocity gradient seen across the cloud is due to rotation, it implies an angular velocity of 3.8×10^{-14} s^{-1}. This would provide only slightly more than 1% of the support needed to balance gravity. Consequently, we conclude that the cloud is gravitationally bound.

3.5. *Ammonia Abundance*

The ammonia abundance is of interest because of considerable uncertainty about how it is formed (e.g., Fehsenfeld et al. 1975; Huntress 1977; Adams, Smith, & Millar 1984; Herbst, DeFrees, & McLean 1987; Hasegawa & Herbst 1993; Shalabiea & Greenberg 1994; Bergin, Langer, & Goldsmith 1995) and because it has been suggested to be an indicator of cloud age (e.g., Suzuki et al. 1992).

Above we found that we could not constrain the ortho/para ratio, which is therefore in the range $\sim 1 \leq Q_{\rm ortho}/Q_{\rm para} \leq 3$, with some uncertainty as to the temperature to use for evaluating $Q_{\rm ortho}/Q_{\rm para}$. For $T_J \simeq 22$ K (see above) and $T_k = 30$ K or plausible higher values it is in the range of 0.9–1. We therefore estimate the total ammonia column density from the para-ammonia column density by multiplying by a factor of ~ 2 for equilibrium chemistry, and ~ 4 for early time chemistry. The total ammonia column density is then 1–3 $\times 10^{16}$ cm^{-2}. Using the smaller dimension (0.67 pc) of the cloud as seen in (1, 1) emission, the ammonia space density is ≤ 5–15×10^{-3} cm^{-3}. Since the gas density was found to be $\geq 10^6$, this implies an ammonia abundance of about ≤ 0.5–1.5×10^{-8}, where the larger number applies to early time chemistry.

In view of the uncertainty about how ammonia is formed, the present chemical models cannot give a confident prediction of $[NH_3]/[H_2]$ as a function of time. All seem to agree that it takes at least 10^6 yr to reach an equilibrium abundance, which is typically on the order of 10^{-7} without depletion. Observations of a variety of sources (e.g., Martin & Barrett 1978; Irvine, Goldsmith, & Hjalmarson 1987; Swade 1989) give abundances of this order. Including depletion can reduce the predicted equilibrium abundance to as low as 10^{-8} (Bergin, Langer, & Goldsmith 1995) or even 10^{-9} (Hasegawa & Herbst 1993), though the latter is achieved only at very long times, on the order of 10^8 yr. Thus it appears from the abundance of NH_3 that NGC 6334 I(N) is younger than $\sim 10^6$ yr or is substantially depleted.

4. DISCUSSION

We have found additional evidence that NGC 6334 I(N) is a massive, cold dense cloud. We find that the mass is at least about 3000 $M_\odot$, which is three times the mass previously estimated. The question of greatest interest concerns the evolutionary state of the massive cloud known as NGC 6334 I(N). We note that the ammonia abundance suggests, on the bases of models of interstellar chemistry, that the cloud is less than 10^6 yr old.

The key question is whether a star has already formed at the core of this cloud. Our observations indicate that the cloud increases in density and temperature towards the center. The temperature increase could, however, be due to compressional heating.

A protostar or the future prospect of a protostar is suggested by the presence of an H_2O maser at the center of the cloud. H_2O masers are associated with the formation of massive stars, perhaps arising even before the onset of nuclear burning. The northernmost H_2O maser in NGC 6334 coincides with the peak of NH_3 emission discussed here. Of the five H_2O masers in the NGC 6334 molecular cloud complex, only this one is not associated with other indicators of star formation, such as OH masers, 69 μm emission, or compact H II regions. This maser is of average intensity and spectral complexity. Extreme conditions of temperature (200–300 K) and density ($\sim 10^{10}$ cm^{-3}) are implied by the H_2O maser. The absence of OH masers and measurable radio continuum emission, along with the simple H_2O spectrum, implies that this region is in an early stage of star formation. The location of the H_2O maser strongly suggests that it lies at the core of a massive molecular clump which is either forming or about to form stars.

At the I position 2′ to the south, H_2 observations made with 20″ resolution (Straw & Hyland 1989) show a peak of emission, with a secondary peak about 1 arcmin north and slightly west at approximately the position of continuum source E (Rodriguez et al. 1982; see Fig. 1 in Gezari 1982). The existence of shocked gas implied by this emission is consistent with gas flowing out from a newly formed star and constrained by the

circumstellar toroid or disk seen in ammonia by Jackson et al. (1988). At the I(N) position, VLA observations show no evidence of a toroid or any other compact source structure in ammonia (J. M. Jackson 1993, private communication). There is some H_2 emission about 1 arcmin west of I(N). If this is indeed associated with I(N), then it would indicate that this source is at a later evolutionary state than proposed but, as it lies in a line with the other H_2 peaks and the outflow from source I (Jackson et al. 1988), it is more likely part of the outflow from source I.

At present, there is little if any evidence for a newly formed star at the core of the I(N) cloud. Additional observations will be required to rule out absolutely the existence of such a star, but present data indicate that a massive pre-stellar collapsing core presages imminent star formation.

We gratefully acknowledge the assistance of the Director and staff of the Canberra Deep Space Communication Complex (Tidbinbilla) and the staff of the Australian National Radio Astronomy Observatory (Parkes). We thank an anonymous referee for helpful comments. Part of this work was performed by the Jet Propulsion Laboratory, California Institute of technology, under contract with the National Aeronautics and Space Administration.

APPENDIX

NOMENCLATURE

The nomenclature for the sources in this complex has become very confused over the years. Cheung et al. (1978) labeled the 1 mm continuum peaks observed with a 65″ beam as I through IV from northeast to southwest. McBreen et al. (1979), who mapped the region at 69 μm, identified five peaks which they independently labeled I through V, also from northeast to southwest. However, their map did not show what Cheung et al. called peak I, so their peak I corresponds to Cheung et al.'s peak II. The other sources in the two maps do not correspond to each other. Gezari (1982), who mapped the north-east region at 400 μm, followed McBreen et al.'s designations and introduced the name I(North) for Cheung et al. peak I. The McBreen/Gezari convention is now generally followed for designating the IR sources (e.g., Loughran et al. 1986; Jackson et al. 1988).

The first OH masers in the region were discovered by Gardner, McGee, & Robinson (1967), who labeled them A (located at McBreen/Gezari peak I) and B (at peak V) in order of strength. H_2O masers were found at both positions by Knowles (1969). Moran & Rodríguez (1980) observed three additional 22 GHz water maser sources and extended the Gardner nomenclature scheme by labeling them C (at peak IV), D (at peak II), and E (at peak I(N)). Rodríguez et al. (1982), who mapped the region at 6 cm wavelength, compounded the confusion by independently designating the 6 cm continuum peaks A through F instead of following the G-designation convention (e.g., Gardner & Whiteoak 1975). Continuum source F (G351.42 + 0.65, maser A) corresponds to IR peak I. Peak I(N) is not seen at 6 cm. In this paper, we consistently use the McBreen/Gezari notation.

REFERENCES

Adams, N. G., Smith, D., & Millar, T. J. 1984, MNRAS, 211, 857
Batrla, W., Matthews, H. E., Menten, K. M., & Walmsley, C. M. 1987, Nature, 326, 49
Bergin, E. A., Langer, W. D., & Goldsmith, P. F. 1995, ApJ, 441, 222
Cheung, L., Frogel, J. A., Gezari, D. Y., & Hauser, M. G. 1978, ApJ, 226, L149
Cheung, A. C., Rank, D. M., Townes, C. H., Knowles, S. H., & Sullivan, W. T., III. 1969, ApJ, 157, L13
Danby, G., Flower, D. R., Kochanski, E., Kurdi, L. Valiron, P., & Diercksen, G. H. F. 1986, J. Phys. B, 19, 2891
Danby, G., Flower, D. R., Valiron, P., Kochanski, E., Kurdi, L., & Diercksen, G. H. F. 1987, J. Phys. B, 20, 1039
Dreyer, J. L. E. 1962, A New General Catalogue of Clusters and Stars (London: Royal Astronomical Society)
Flower, D. R., Offer, A., & Schilke, P. 1990, MNRAS, 244, 4P
Fehsenfeld, F. C., Lindinger, W., Schmeltekopf, A. L., Albritton, D. L., & Ferguson, E. E. 1975, J. Chem. Phys., 62, 2001
Forster, J. R., Whiteoak, J. B., Gardner, F. F., Peters, W. L., & Kuiper, T. B. H. 1987, Proc. Astron. Soc. Australia, 7, 189 (FWGPK)
Gardner, F. F., McGee, R. X., & Robinson, B. J. 1967, Australian J. Phys., 20, 309
Gardner, F. F., & Whiteoak, J. B. 1975, MNRAS, 173, 131
Gezari, D. 1982, ApJ, 259, L29
Gómez, Y., Rodríguez, L. F., Garay, G., & Moran, J. M. 1991, ApJ, 377, 519
Green, S. 1980, J. Chem. Phys., 73, 2740
Guilloteau, S., Wilson, T. L., Martin, R. N., Batrla, W., & Pauls, T. A. 1983, A&A, 124, 323
Hasegawa, T. I., & Herbst, E. 1993, MNRAS, 261, 83
Herbst, E., DeFrees, D. J., & McLean, A. D. 1987, ApJ, 321, 898
Ho, P. T. P., Barrett, A. H., Myers, P. C., Matsakis, D. N., Cheung, A. C., Chiu, M. F., Townes, C. H., & Yngvesson, K. S. 1979, ApJ, 234, 912
Huntress, W. T., Jr. 1977, ApJS, 33, 495
Irvine, W. M., Goldsmith, P. F., & Hjalmarson, A. 1987, in Summer School on Interstellar Processes, ed. D. J. Hollenbach & A. A. Thronson (Dordrecht: Reidel), 561
Jackson, J. M., Ho, P. T. P., & Haschick, A. D. 1988, ApJ, 333, L73
Knowles, S. H., Mayer, C. H., Sullivan, W. T. III, & Cheung, A. C. 1969, Science, 166, 221
Kuiper, T. B. H. 1994, ApJ, 433, 712
Kuiper, T. B. H., Peters, W. L., III, Forster, J. R., Gardner, F. F., & Whiteoak, J. B. 1987, PASP, 99, 107
Kuiper, T. B. H., Rodriguez Kuiper, E. N., Dickinson, D. F., Turner, B. E., & Zuckerman, B. 1984, ApJ, 276, 211
Loughran, L., McBreen, B., Fazio, G. G., Rengarajan, T. N., Maxson, C. W., Serio, S., Sciortino, S., & Ray, T. P. 1986, ApJ, 303, 629
Mangum, J. G., & Wootten, A. 1994, ApJ, 428, L33
Martin, R. N., & Barrett, A. H. 1978, ApJS, 36, 1
McBreen, B., Fazio, G. G., Stiev, M., & Wright, E. L. 1979, ApJ, 232, L183
Menten, K. M. 1991, in Atoms, Ions, and Molecules: New Results in Spectral Line Astrophysics, ed. A. D. Haschick & P. T. P. Ho (San Francisco: ASP), 199
Menten, K. M., & Batrla, W. 1989, ApJ, 341, 839
Moran, J. M., & Rodriguez, L. F. 1980, ApJ, 236, L159
Morris, M., Zuckerman, B., Palmer, P., & Turner, B. E. 1973, ApJ, 186, 501
Neckel, T. 1978, A&A, 69, 51
Raimond, E., & Eliasson, B. 1969, ApJ, 155, 817
Rodríguez, L. F., Cantó, J., & Moran, J. M. 1982, ApJ, 225, 103
Schwartz, P. R., Bologna, J. M., & Waak, J. A. 1978, ApJ, 226, 469
Shalabiea, O. M., & Greenberg, J. M. 1994, A&A, 290, 266
Straw, S. M., & Hyland, A. R. 1989, ApJ, 342, 876
Stutzki, J., & Winnewisser, G. 1985a, A&A, 144, 1
———. 1985b, A&A, 148, 254
Suzuki, H., Yamamoto, S., Ohishi, M., Kaifu, N., Ishikawa, S., Hirhara, Y., & Takano, S. 1992, ApJ, 392, 551
Swade, D. A. 1989, ApJS, 71, 219
Walmsley, C. M., & Ungerechts, H. 1983, A&A, 122, 164
Wilson, T. L., Downes, D., & Bieging, J. 1979, A&A, 71, 275
Ziuris, L. M., Martin, R. N., Pauls, T. A., & Wilson, T. L. 1981, A&A, 104, 288